Mapping the X-Press Pearl ship disaster oil spill drift patterns in the Indian Ocean using Sentinel 1 SAR time series

Welikanna D.R [1*]

[1] *Department of Surveying and Geodesy, Faculty of Geomatics, University of Sabaragamuwa, Sri Lanka*

[*]drw@geo.sab.ac.lk

Abstract *X-Press Pearl container tanker ship disaster is considered the biggest marine disaster to have occurred in the Indian ocean. Other than the identification of the resulting oil spill, the drift patterns and the temporal evolution of the oil film is important to assess the damages caused by the incident. The study employs a recently proposed damping ratio (DR) index in combination with a data-driven GMM-EM clustering method optimized by stochastic ordering to investigate the drift patterns caused by the disaster. The inclusion of GMM based clustering principles and the optimization is a novel approach proposed in this study. It goes on to show that the use of GMM based methods provide reasonable class separability to correctly determine the* $\sigma_{VV}^{0,sea}(\theta)$ *in order to define the oil spill associated ocean contrast using DR. A series of 10 Sentinel 1 C band VV polarized SAR images capturing the Xpress Perl shipwreck oil spill from May 27, 2021, to September 24, 2021, were employed. The detected oil slick shows a strong presence, especially on May 27th, June 8th and 20th, July 26th, and August 31st, with approximate patch widths of 0.81 km, 2.23 km, 6.24 km, 2.24km, and 1.51 km, respectively. On average, during the time of the analysis, the oil patch had occupied a range > 0.5 km, other than in the case where it settled down on September 24th, 2021. The DR values for the oil class ranged from 4 to 8 on average. As a whole, the X-Press Perl ship wreck can be seen causing oil pollution throughout the period of four months in the west coast of Sri Lanka.*

Keywords: Damping ratio (DR), Ship wreck Oil spills, Oil spill remote sensing, synthetic aperture radar (SAR), K-Means, GMM

Introduction

Sri Lanka is geographical located at the center of the Indian Ocean. It is home to the only commercial deep-water port ("Colombo") in South Asia with a high marine value (Osmund Bopeararchchi, 2002). Due to the large maritime activities in the Indian Ocean close to Sri Lanka, oil spills can be considered as a regular geographic phenomenon of concern (Table 1) (Centre for Environmental Justice, 2022; Marine Traffic, 2021). The increasing trend in the oil spill occurrences need reliable monitoring for its extent, form and the drift patterns. This is

highly possible with the use of remote sensing techniques (Rajendran et al., 2021; Rao et al., 2022).

Table 1- Notable Shipwrecks and possible oil spills reported in the Indian Ocean (2020-2021)

Date	Ship	Shipwreck Incident
3rd September 2020	**MT New Diamond**	Oil Spill formation
20th May 2021	**X-Press Pearl**	Major Oil spill disaster
25th June 2021	**MSC Messina**	Oil Spill formation

X-Press Pearl ship disaster among the others (Figure 1) is considered the weightiest marine disaster to have occur in the history of the Indian Ocean. This study concentrates on its oil spill formation and drift. We employ a new derivation of Damping Ratio (DR) to detect the oil spill and its drift. A combine use of Gaussian Mixture Model (GMM) based clustering with stochastic ordering is employed to derive the DR to detect and map the oil spill caused by the X-Press Pearl ship wreck (Welikanna & Jin, 2024).

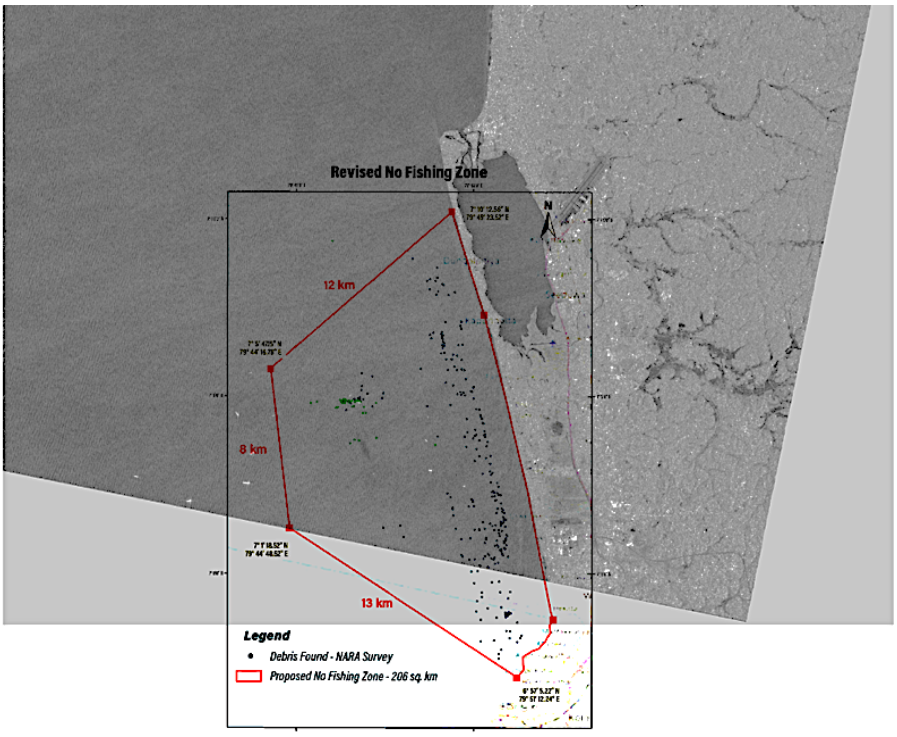

Figure 1: Shows the first existence of the ship wreck oil spill detected by Sentinel 1 C band SAR VV polarization on 20210527 over the west coast of Sri Lanka, and the Debris survey and mapping conducted by the NARA.

Backscattered energy from the sea surface measured by synthetic aperture radar (SAR) is a useful source for identifying sea wind patterns, ships, and oil spills (Brekke & Solberg, 2005;

Fiscella et al., 2000). Oil spills on sea surfaces smooths the water, suppresses the capillary and gravity waves reducing the returning radar signal strength. They appear dark in SAR images and can be detected by using both backscatter intensity (dB) or normalized radar cross section (NRCS) (Fiscella et al., 2000; Johansson, 2022). DR is a simple and emerging methodology that can be utilized to detect oil spills and its formation speedily (Jones, 2023a; Jones and Holt, 2018a; Quigley et al., 2023a).

Methodology

DR measures the variation of energy in a SAR image. As a consequence, DR can provide details of the scattering properties related to different materials. DR is defined by the following equation:

$$DR = \frac{\sigma_{VV}^{0,sea}(\theta)}{\sigma_{VV}^{0}(\theta)} \quad (1)$$

Where $\sigma_{VV}^{0,sea}(\theta)$ and $\sigma_{VV}^{0}(\theta)$ are the backscatter intensity of the open sea water and the measured total intensity at θ incidence angle, respectively. NRCS linear units can be used in the equation effectively. Low DR values represent stronger scattering, while weak scattering is followed by a higher DR. DR is an emerging and simple approach to map oil spills. TDR calculation for oil spills is detailed by the following studies (Brekke and Solberg, 2005; Jones, 2023a; Quigley et al., 2023a)(A. S. Solberg et al., 2004; Jones and Holt, 2018a; Richard O. Duda et al., 2001; Shen et al., 2022; V. Wismann et al., 2010). The difficulty of deriving DR is to correctly determine the $\sigma_{VV}^{0,sea}(\theta)$. To address this, we propose a novel method using, GMM based EM clustering principle with stochastic ordering to determine $\sigma_{VV}^{0,sea}(\theta)$ and subsequently the DR (Welikanna & Jin, 2024). Before calculating the DR, we investigate the wind patterns aiding the oil spill drift (Figure 2). Wind speeds and directions were derived using Ground Range Detected (GRDH) time series images of Sentinel 1 and the ESA SNAP 9.0.0 Ocean application tool (A. S. Solberg et al., 2004; Richard O. Duda et al., 2001; Shen et al., 2022).

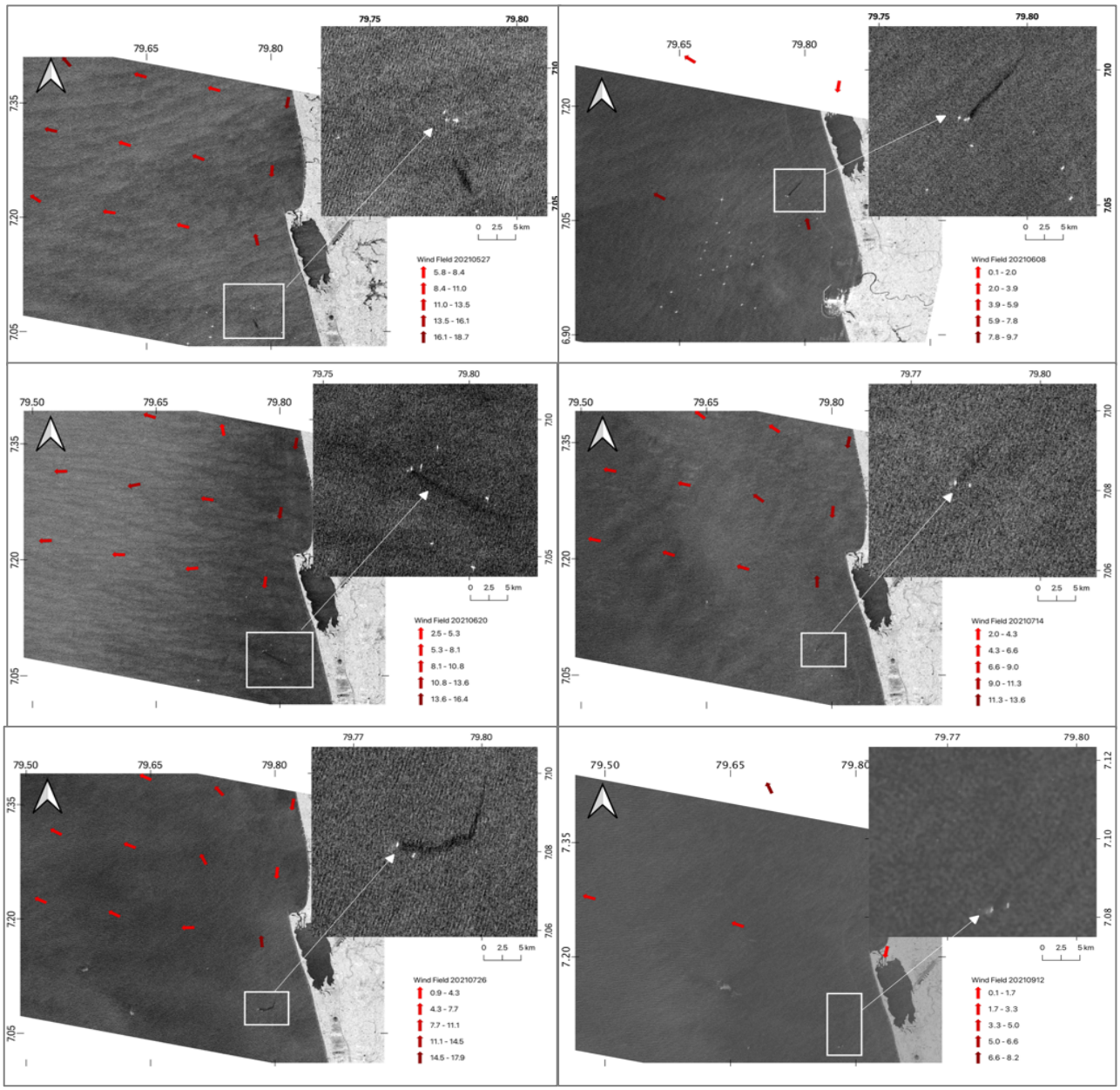

Figure 2: Behavioral change of the oil spill (Backscatter intensity) foot print with the respective wind fields (wind speeds and directions on 20210527, 20210608, 20210620, 20210714, 20210726 and 20210912) derived using the SAR GRDH images

The data-driven stochastic ordering proposed in the study is determined by using the pixel distribution inherent to shipwreck oil spills. It enforces the correct determination of class values for DR. It is a simple mathematical condition realized by analyzing the pixel dB variation along the transects, as shown in Figure 3 (Welikanna & Jin, 2024).

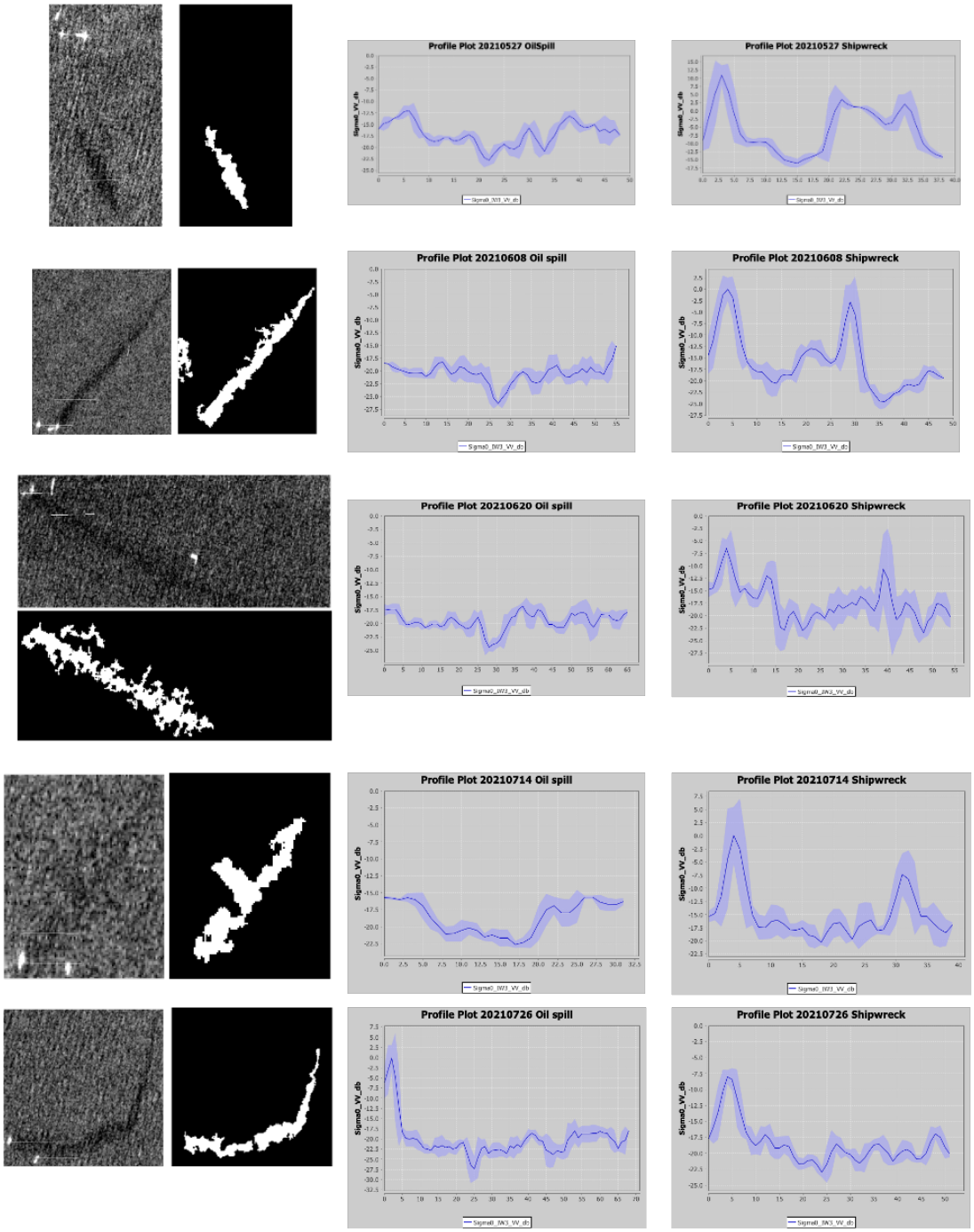

Figure 3: Extracted oil spills and the Oil spill and Shipwreck back scatter (dB) profiles along the identified transect. Oil spills were extracted using the ESA SNAP SAR applications oil spill detection tool.

The data driven stochastic ordering governing the NRCS values in any given spatial neighborhood $\mathcal{N}$. For shipwreck oil spill this relation can be represented as follows:

$$NRCS_{\omega_1} < NRCS_{\omega_2} < NRCS_{\omega_3} \quad \forall \mathcal{N} \tag{2}$$

The high-confidence water pixel parameter needed for the DR, is then determined as follows:

$$\sigma_{VV}^{0,sea}(\theta) = NRCS_{\omega_2} \tag{3}$$

The use of clustering avoids high-confidence clean water masks and promotes high-confidence clean-sea pixel identification ($\sigma_{VV}^{0,sea}(\theta)$). For the original pixel distribution determination, we employed the GMM after removing the speckle using the GAMMA-MAP filter. The initial parameters for each cluster in the GMM were determined by using the K-means cluster initialization. A polynomial fitting is carried out to define the class mean values. Finally, to optimize the GMM parameters, the EM clustering mechanism was used. The overall methodological work flow is shown below(Welikanna & Jin, 2024) .

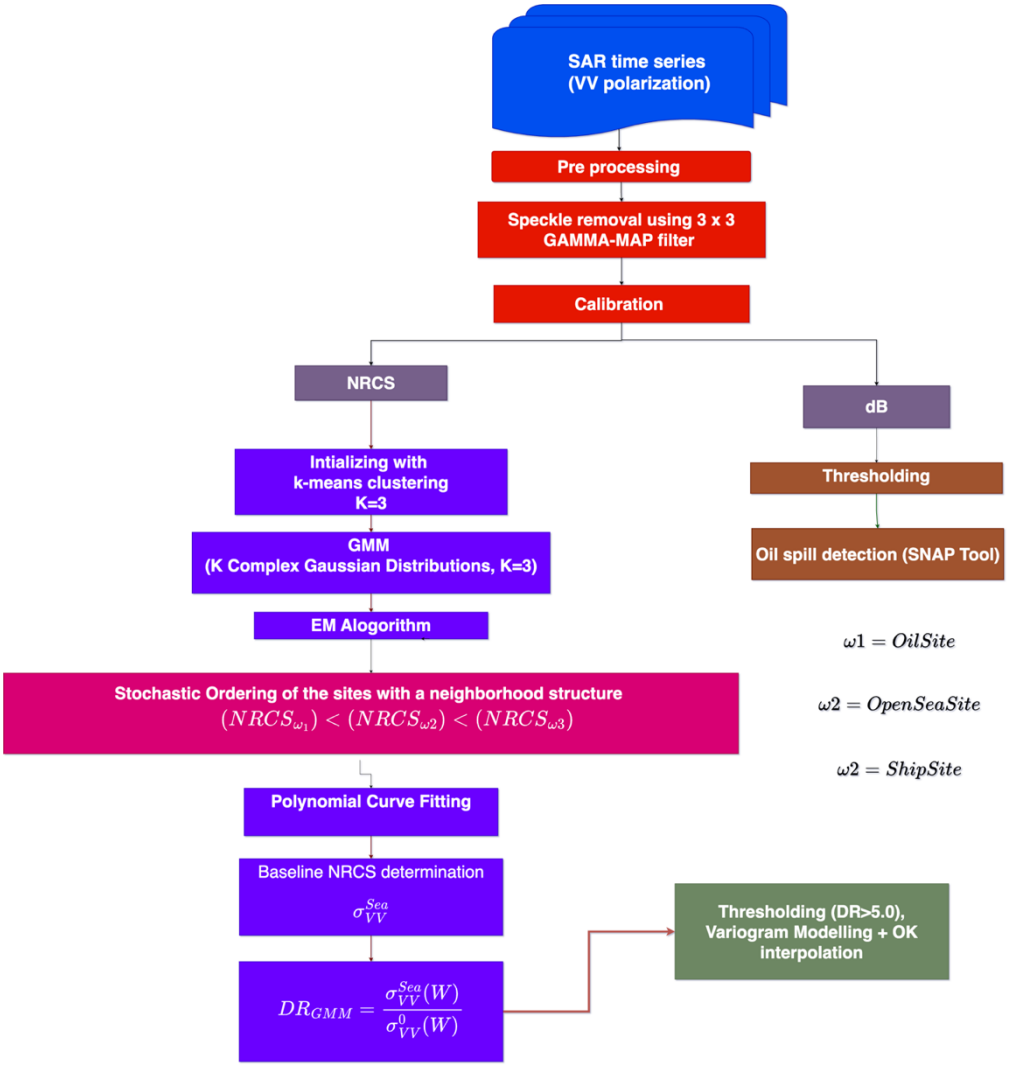

Figure 4: The overall methodological flow

Results and Discussion

Sentinel 1 Level-1 Single Look Complex (SLC) VV polarized images capturing the Xpress Perl shipwreck oil spill from May 27, 2021, to September 24, 2021 were employed (for the purpose of the paper results from 20210527, 20210608, 20210726 and 20210831are reported). The cluster locations from the GMM based EM under the stochastic ordering, respective PDFs, (for 3 classes) and the DR images computed using the GMM mean values for the $\sigma_{VV}^{0,sea}(\theta)$ are presented in Figure 5. The results of the clustering are shown in Table 5. A stronger radar BS (ship) is indicated by a DR value close to 0, while a higher value indicates a strong contamination by oil. The deduced DR values for the oil class ranged from 4 to 8. The PDF plots show the marginal differences in the distributions for the oil and open sea classes. A nominal standard deviation for the two classes denotes homogeneity.

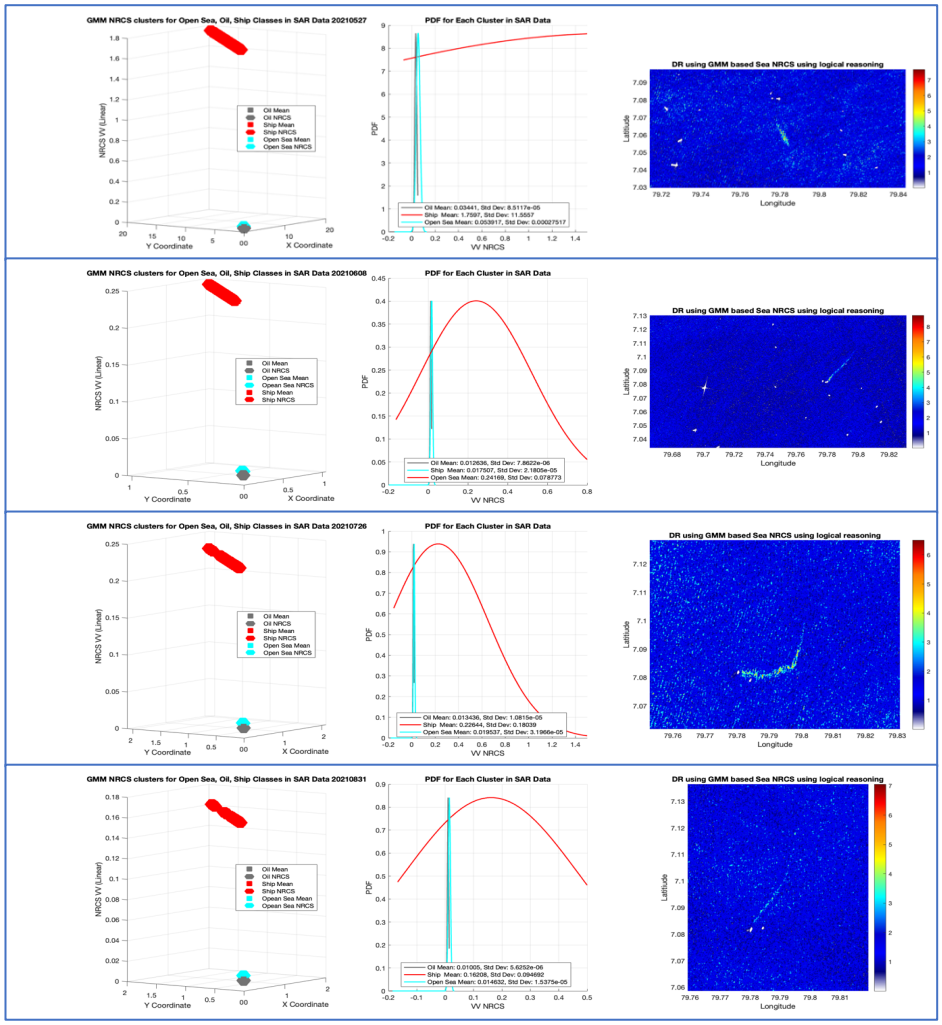

Figure 5: GMM clustering results using SAR NRCS, the placement of the clusters in 3D feature space, respective PDF and the DR images derived using the GMM mean for the $\sigma^{sea}(\theta)$

Table 5. Initial K-mean cluster means and EM based optimized GMM based cluster means, class mixing proportions, fitted polynomial constants and their standard deviations (SD)

Date/Cluster		Initial K-Means	GMM Means	Mixing proportions	Polynomial constants	SD
20210527	Oil	0.0404	0.0344	0.748812	0.0350	0.0087
	Open Sea	5.0686	0.0539	0.248582	0.0653	0.0116
	Ship	14.0450	1.7597	0.002606	2.1975	3.4392
20210608	Oil	0.0121	0.0126	0.660995	0.0124	0.0027
	Open Sea	0.0198	0.0175	0.336754	0.0212	0.0031
	Ship	0.700	0.2417	0.002251	0.6143	1.0581
20210726	Oil	0.0127	0.0134	0.678691	0.0128	0.0030
	Open Sea	0.0215	0.0195	0.019500	0.0227	0.0038
	Ship	1.4264	0.2264	0.000716	0.4356	0.4296
20210831	Oil	0.0113	0.0101	0.732771	0.0099	0.0021
	Open Sea	0.4639	0.0146	0.266385	0.0168	0.0027
	Ship	1.6206	0.1621	0.000844	0.0664	0.3065

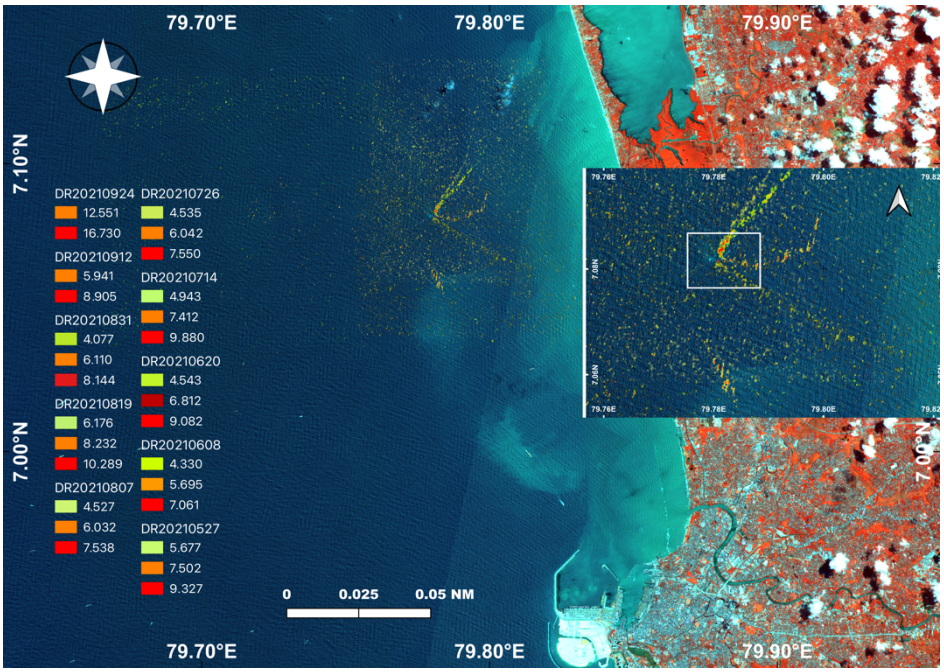

Figure 6: The DR based time series oil spill from the X-Press Perl ship, superimposed over the Sentinel 2 image acquired on 19th July 2021. The half-submerged ship is visible in the false color composite (R- B8, G-B3 and B- B2). The times series DR propagation suggests an anticlockwise movement from south to NE. No fishing zone and the field pollutant constituents suggests a close correlation.

The resulting DR images were segmented to extract the oil spill using thresholds representing possible oil portions in the higher ends of the DR (>4.0). For the respective DR image, these threshold values and the temporal variation of the oil spills are shown in Figure 6. The NARA-based site surveys have demarcated the no-fishing zone due to the oil spill and the debris flow.

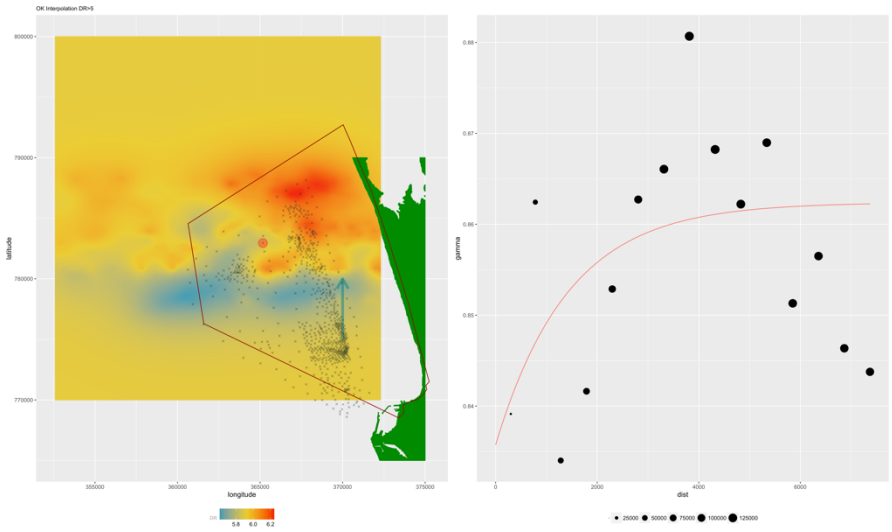

Figure 7:. The Ordinary kriging (OK) results and the respective spherical variogram model used to construct the spatial correlation structure. The NW debris movement is highlighted from the OK for the DR values in the range >5.0. The whole time series DR values were used for the interpolation.

The high DR values (> 5.0) representing the significant oil damping of the sea water were modelled for its drift using variograms. A spherical variogram was found to model the time series oil spill of the X-Press Perl, as shown in Figure 7. The partial sill was reached at 0.8357 (DR) at a range of 1431.616m. The nugget value stayed at 0.0266 (DR). Ordinary Kriging (OK) interpolation was performed to predict the overall oil spill drift during the period of the study from May 2021 to September 2021. The range suggests spatial dependence of DR values extends up to a distance of 1.431Km. As we have considered the DR values pertaining to the 5 months of the year 2021. The relatively high partial sill (0.8 DR) suggests a strong spatial structure for the shipwreck oil spill. The nugget value of 0.2 (DR) suggests that, other than the spatial autocorrelation structure, variability at very short distances exists with the oil spill. This could be due to factors like winds, local variations in the environment, or measurement noise. As shown in Figure 7, the higher DR ranges predicted by OK are along the coast where the no fishing zone was demarcated (Welikanna & Jin, 2024).

Conclusion and recommendation

The X-Press Pearl shipwreck was stable at the same location while it completed the sank on the seabed, roughly 21m by June 17, 2021, leaving the castle and a few cranes visible (De Vos et al., 2022). The average wind direction was N-NW, with the highest speeds around the range of 13 m/s and the lowest around 0.1 m/s (Table 3). High wind speeds were identified on July 14 and August 7, 2021, making oil spill detection difficult. The slick subjected to this study shows disorganized oil spill behavior from the time of its existence. The detected oil slick shows a strong presence, especially on May 27th, June 8th and 20th, July 26th, and August 31st (Figure 2, 3 and 5), with approximate patch widths of 0.81 km, 2.23 km, 6.24 km, 2.24km, and 1.51 km, respectively. On average, during the time of the analysis, the oil patch had always occupied a range > 0.5 km, other than in the case where it settled down on September 24th, 2021. The DR images resulting from the GMM clustering show the oil slick behavior to be similar to the analysis done using the oil spill detection tools in SNAP on a dB scale. The main difficulty in deriving DR is identifying the most probable value of the sea site $\sigma^{sea}(\theta)$ as the class representative NRCS. In this study, clustering principles to derive DR are proposed by using GMM-based EM clustering with K-means initialization. Following the GMM clustering, first-order polynomials were employed to realize consistent class representations by using the polynomial constant as the baseline NRCS for each class. Additionally, using the spatial autocorrelation structure of the oil spill with DR > 5.0, we have interpolated the results to produce the overall drift of the oil spill for the 4-months period. The maps created by SAR DR would be vital evidence to quantify the marine damage and necessary compensation claims currently in the proceedings(Welikanna & Jin, 2024).

References

A. S. Solberg, C. Brekke, & R. Solberg. (2004). Algorithms for oil spill detection in Radarsat and ENVISAT SAR images. *Geoscience and Remote Sensing Symposium, 2004. IGARSS '04. Proceedings*.

Brekke, C., & Solberg, A. H. S. (2005). Oil spill detection by satellite remote sensing. In *Remote Sensing of Environment* (Vol. 95, Issue 1, pp. 1–13). https://doi.org/10.1016/j.rse.2004.11.015

Centre for Environmental Justice. (2022). *X-PRESS PEARL: A "NEW KIND OF OIL SPILL" A TOXIC MIX OF PLASTICS AND INVISIBLE CHEMICALS*. www.ipen.org

De Vos, A., Aluwihare, L., Youngs, S., Dibenedetto, M. H., Ward, C. P., Michel, A. P. M., Colson, B. C., Mazzotta, M. G., Walsh, A. N., Nelson, R. K., Reddy, C. M., & James, B. D. (2022). The M/V X-

Press Pearl Nurdle Spill: Contamination of Burnt Plastic and Unburnt Nurdles along Sri Lanka's Beaches. *ACS Environmental Au*, *2*(2), 128–135. https://doi.org/10.1021/acsenvironau.1c00031

Fiscella, B., Giancaspro, A., Nirchio, F., Pavese, P., & Trivero, P. (2000). Oil spill detection using marine SAR images. *International Journal of Remote Sensing*, *21*(18), 3561–3566. https://doi.org/10.1080/014311600750037589

Johansson, M. (2022). *Disaster Assessment Using Synthetic Aperture Radar Part 3-Oil Spill Detection*.

Jones, C. E. (2023). An automated algorithm for calculating the ocean contrast in support of oil spill response. *Marine Pollution Bulletin*, *191*. https://doi.org/10.1016/j.marpolbul.2023.114952

Jones, C. E., & Holt, B. (2018). Experimental L-band airborne SAR for oil spill response at sea and in coastal waters. *Sensors (Switzerland)*, *18*(2). https://doi.org/10.3390/s18020641

Marine Traffic, X.-P. Pearl. 2021. (2021). *https://www.marinetraffic.com/en/ais/details/ships/shipid:6450863/mmsi:563118200/imo:9875343/vessel:X_PRESS_PEARL*.

Osmund Bopeararchchi. (2002). Archaeological evidence on shipping communities of Sri Lanka. Ships and the Development of Maritime Technology in the Indian Ocean. In *Ships and the Development of Maritime Technology on the Indian Ocean* (1st ed., Vol. 1). Routledge.

Quigley, C., Johansson, A. M., & Jones, C. E. (2023). An Investigation on the Damping Ratio of Marine Oil Slicks in Synthetic Aperture Radar Imagery. *IEEE Journal of Selected Topics in Applied Earth Observations and Remote Sensing*, *16*, 5488–5501. https://doi.org/10.1109/JSTARS.2023.3285145

Rajendran, S., Vethamony, P., Sadooni, F. N., Al-Kuwari, H. A. S., Al-Khayat, J. A., Seegobin, V. O., Govil, H., & Nasir, S. (2021). Detection of Wakashio oil spill off Mauritius using Sentinel-1 and 2 data: Capability of sensors, image transformation methods and mapping. *Environmental Pollution*, *274*. https://doi.org/10.1016/j.envpol.2021.116618

Rao, V. T., Suneel, V., Alex, M. J., Gurumoorthi, K., & Thomas, A. P. (2022). Assessment of MV Wakashio oil spill off Mauritius, Indian Ocean through satellite imagery: A case study. *Journal of Earth System Science*, *131*(1). https://doi.org/10.1007/s12040-021-01763-3

Richard O. Duda, Peter E. Hart, & David G. Stork. (2001). *Pattern Classification* (Second Edition, Vol. 2). Wiley.

Shen, H., Jiang, M., Li, J., Zhou, C., Yuan, Q., & Zhang, L. (2022). Coupling Model-and Data-Driven Methods for Remote Sensing Image Restoration and Fusion: Improving physical interpretability. *IEEE Geoscience and Remote Sensing Magazine*, *10*(2), 231–249. https://doi.org/10.1109/MGRS.2021.3135954

V. Wismann, M. Gade, W. Alpers, & H. Huhnerfuss. (2010). Radar signatures of marine mineral oil spills measured by an airborne multi-frequency radar. International Journal of Remote Sensing, 19(18), 3607–3623. doi-10.1080:014311698213849. *International Journal of Remote Sensing*, *19*(18).

Welikanna, D. R., & Jin, S. (2024). A data driven oil spill mapping using GMM clustering and damping ratio on X-Press Pearl ship disaster in the Indian Ocean. *Marine Pollution Bulletin*, *203*. https://doi.org/10.1016/j.marpolbul.2024.116392